Kinematic Control of a Mobile Robot Performing Manufacturing Tasks on Non-Planar Surfaces

Joshua Qualls, Stephen Canfield, Alexander Shibakov

Abstract:

Mobile robotic systems are becoming viable technologies for automating manufacturing processes in fields that traditionally have seen little automation. Such fields include pipeline construction, green energy development, infrastructure and shipbuilding. To operate in these environments, the mobile robotic platform must provide controlled motion of a manufacturing toolset over the surface of a structure which is generally non-planar. One such example is welding a seam along a non-flat ship hull where the surface may consist of sections resembling common geometric shapes such as cylinders or spheres and the tool must follow a path defined by the weld seam. This paper will present a kinematic control approach applicable to one mobile robot topology performing a task on a cylindrical surface. This method is readily generalized to other robot topologies or surface geometries. The method is based on a kinematic model that predicts the robot motion and configuration joint parameters while on a non-planar surface with the desired motion prescribed in local tool space. The effort is motivated by a practical application of welding on steel hulls or other surfaces and the results will be compared with these empirical experiences. A discussion of how these results can be used to guide future design of mobile robot platforms for manufacturing is provided.

Keywords: *kinematic, control, mobile robot, manufacture, non-planar surface*

1. Introduction

The development of mobile robot systems is growing at a rapid pace. These systems are being investigated in arenas including surveillance, agriculture, medical and manufacturing to name a few. In manufacturing, mobile robots may provide an avenue to bring increased automation to unstructured manufacturing environments in which the manufactured device is large and/or must be constructed on-site rather than in a factory. Examples of unstructured manufacturing environments include erecting civil structures, constructing energy producing facilities, tanks, pipelines, or shipbuilding. Early research on mobile robot manufacturing applications has shown promise in automating tasks such as welding and inspection, [1, 2]. These applications require the ability to follow a path while performing the automated task at hand. Task planning and control rely on a suitable kinematic and/or dynamic model of the mobile system. It has been demonstrated the kinematics of vehicles is dependent on the terrain and as such must be considered in the modeling process [3–5]. These studies generally consider surface material properties rather than the geometric properties which may directly impact friction and potential slipping. In manufacturing, the surfaces are generally metal which tend to be more isotropic than ground terrain. However, geometric properties are important if the manufacturing shapes are non-planar. The vast majority of kinematic models demonstrated in the literature assume the robot system is operating on planar surfaces [6–9]. In practice, the mobile robot often operates on a manufactured surface generally consisting of non-planar surfaces. Most kinematic control models assume the surface is locally planar. To a much smaller extent, kinematic models for mobile robots have been developed that can account for non-planar geometric surfaces [10–17]. Of these papers, the most common technical approach to building the model is to generate a state-specific representation of the interaction between the wheel contact and the ground, [9], or to employ a more general relationship describing the kinematic behavior of contact between the wheel and surface, while retaining the classic kinematic assumptions of no relative motion along a common normal, [11]. Several papers build on generalized contact equations proposed and developed by Montana, [18], resulting in a set of five ordinary differential equations describing the propagation of the contact point between two general surfaces. This approach has been applied to mobile robot modeling by several authors including [12–14], where the most common application of these models is to evaluate specific mobile robot topologies that can eliminate or reduce wheel slipping when traveling over non-planar terrain, [15–17]. While little work has been conducted on applications regarding manufacturing-specific tasks, these tasks pose an impact on the model development. The geometric properties of the surfaces are known a-priori and in many cases consist of simple Boolean shapes. Manufacturing tasks require the robot to coordinate a tool function while following a prescribed path, with coordinates specified in tool space, and place specific tolerances on the tool motion. Finally, the manufacturing task is known ahead of time and can be simulated. This allows an evaluation of the planar assumption and determines

the range of manufacturing operations suitable for a more simplistic planar-based kinematic model as opposed to a detailed, non-planar model.

2. Approach

A kinematic model of the robot system suitable for non-planar surfaces is constructed in this section. This model is developed in the context of a mobile manufacturing robot capable of climbing metal surfaces in order to conduct common tasks associated with manufacturing, [1]. Such a model implies that the robot is primarily traveling at lower velocities associated with tasks such as welding, machining, or cutting. It also implies that the surface features can be assumed more isotropic (material properties) or known a priori (geometrical properties). In manufacturing or inspection operations, the task is generally defined as a specified path or trajectory along which a tool must travel while conducting welding, cutting or similar type functions. As an example, consider the robot in Figure 1 in which the mobile robot is simultaneously cleaning and inspecting the wall of a tank for pitting, corrosion, or cracks. This scenario is representative of a broad variety of manufacturing tasks that could be performed by mobile robots. The robot in this example is operating on a surface which is predominantly cylindrical in shape; with many manufacturing surfaces consisting of a relatively small number of uniform geometric shapes. Therefore, path following along simplistic geometric surfaces will serve as the representative scenario for this paper. The improved kinematic model of the robot system can be used in several ways, such as a tool for design and development of these robots, to serve as a tool in planning, manufacturing and maintenance tasks, or to aid in navigation during operation. This model will provide a better predictor of robot kinematic motion on a non-planar surface and will be demonstrated for a cylindrical climbing surface; although the method can be applied to any other surface by defining the surface curvature, metric and torsion.

In the traditional mobile robot model for a differential drive system, a set of differential equations are given in the robot kinematics that describe propagation of the robot platform frame position and orientation in time as,

$$\begin{Bmatrix} \dot{x} \\ \dot{y} \\ \dot{\theta} \end{Bmatrix} = \mathbf{J} \begin{Bmatrix} \dot{\theta}_l \\ \dot{\theta}_r \end{Bmatrix} \tag{1}$$

where $\{\dot{x}, \dot{y}, \dot{\theta}\}^T$ describes the planar motion of the robot in the local robot frame given, $\{\dot{\theta}_l\, \dot{\theta}_r\}^T$ the vector of inputs for the differential drive system (input wheel rotations) and $\mathbf{J}$ the system Jacobian, which is independent of robot configuration parameters, $\{\theta_l\, \theta_r\}^T$. The model in Equation 1 is generally developed by assuming pure roll and no slip which can be used to describe the motion of the contact points between the ground and wheel surfaces as,

$$\dot{\mathbf{U}}_{W_i} = \mathbf{R}_r^{W_i} \begin{Bmatrix} \dot{\theta}_i r_w \\ 0 \end{Bmatrix}, \ i = l, r, \tag{2}$$

$$\dot{\mathbf{U}}_{S_i} = \mathbf{R}_r^{S_i} \left(\begin{Bmatrix} \dot{x} \\ \dot{y} \end{Bmatrix} + \dot{\theta} \hat{k} \times \mathbf{d}_i \right), \ i = l, r, \tag{3}$$

with $\mathbf{U}_{W_i}$ and $\dot{\mathbf{U}}_{S_i}$ representing the velocity of the contact point as 2d vectors residing in the plane tangent to the wheel and surface respectively, r_w the wheel radius and, $\mathbf{d}_i$ the vector from the robot frame to the contact point and subscripts W and S identify the contact point for the wheel or surface respectively. Further, the subscript i will be used throughout this paper to identify the wheel for which the equations are written; for example the left wheel, right wheel or castor wheel ($i = L, R, C$). The contact point velocities $\mathbf{U}_{W_i}$ and $\dot{\mathbf{U}}_{S_i}$ are described in the wheel and surface frames respectively with $\mathbf{R}_r^{W_i} \mathbf{R}_r^{S_i}$ projections from the robot frame to wheel and surface frame. These equations can be integrated in time to track the robot location. Furthermore, when considering robot motion on a planar surface, any set of frames depending on the configuration coordinates could remain constant since the location of the contact point between the wheels and the surface is assumed to be constant relative to the robot.

When considering motion on non-planar surfaces, the Jacobian, $\mathbf{J}$, becomes a function of $\mathbf{q}$, containing the traditional configuration coordinates plus a series of geometry dependent variables that describe the configuration of the robot chassis relative to the surface through each of the wheels (see for example Figure 2). The contact velocities are functions of surface conditions and the $\mathbf{q}$ update must be consistent with the surface geometry. It should be noted that one of the complicating factors in the non-planar case is that it is non-obvious to define a consistent and desired velocity state. For the planar case, this is straightforward; define $\dot{\mathbf{q}}$ or use the no-slip condition to define the robot frame velocity through $\dot{x}$ and $\dot{\theta}$. In the non-planar case, the robot frame velocity must be defined consistent with kinematic and geometric conditions. A method to address these issues consists of the following steps. Starting from a known location,

Fig. 1. Mobile Robot Performing Surface Inspection

an instantaneous kinematic model of the robot is constructed assuming a temporary state of no slip. This is used to find the relative velocities between the wheels and climbing surface for a consistent set of input velocities. Next, a set of first order differential equations, called contact equations, are employed to define the velocity of the contact points in the wheel and surface frames based on these relative velocities. The contact equations are integrated in time to update the location of the robot on the climbing surface. Finally, the robot configuration parameters are updated in time by satisfying the robot kinematic constraints and new wheel locations.

2.1. Mobile Robot Kinematics

In the remainder of this paper an upright circular cylinder will serve as the reference climbing surface while the robot architecture will be based on a differential steer system with three wheels; left, right, and caster. The left and right wheels are driven by independent motors and the caster having a passive revolute joint. The robot under consideration is capable of climbing on ferrous surfaces as discussed in [1]. In addition, the robot will contain one passive suspension revolute joint aligned centrally in the longitudinal direction of the robot. A schematic of this robot is shown in Figure 2.

An instantaneous model of the robot is constructed with the robot represented as three in-parallel serial chains called wheel chains, connecting the robot chassis to the surface. The contact point for each wheel is modeled as a spherical connection with ground (providing an instantaneous pure roll no slip condition) and the wheel axle modeled as a revolute.

The suspension member is part of the left wheel chain and modeled as another revolute in this chain. Similarly, the passive caster joint found in the caster wheel chain is also modeled as a revolute. This treats the robot as an instantaneous holonomic in-parallel system with two 5 degree of freedom (dof) chains for the left and caster wheel and a 4 dof chain for the right wheel.

A series of frames are then defined to represent the path from the cylinder inertial frame, $\{I\}$, through each wheel contact point to the local robot frame, $\{r\}$, for each of the three wheels labeled L, R and C as shown in Figures 2 and 3 with each wheel defined through the use of the subscript i. For each wheel, the first two frames of the wheel chain are located at the contact point, one defined on the climbing surface $\{S_i\}$ and one defined on the robot wheel $\{W_i\}$. Frames $\{S_i\}$ and $\{W_i\}$ are defined in a manner allowing the z axis to reside along the outward normal to the surface and wheel following the method in [13], as shown in Figure 3. Next, a set of frames, from $\{0_i\}$ to $\{4_i\}$ for the left and caster wheel ($i=L, C$) and from $\{0_i\}$ to $\{3_i\}$ for the right wheel ($i=R$) are constructed to define the kinematics of each wheel chain. The first three frames $\{0_i\}$ to $\{2_i\}$ model the contact point instantaneously as a spherical joint assuming no slip, the next frame $\{3_i\}$ defines rotation of the wheel about its axis, and remaining frames define caster rotation $\{4i\}$, $i=C$, and one degree of freedom suspension $\{4_i\}$, $i=L$. Finally, a common frame for the robot, $\{r\}$ is located on the chassis as shown in Figure 3. The frames are based on Denavit and Hartenberg notation, [19], and are shown in Figure 2 (note an extra fixed rotation is required to bring frame $\{4\}$ for the left wheel in alignment with frame $\{r\}$ of the robot chassis). The configuration parameters for each chain are identified as $\theta_{1-5,L}, \theta_{1-5,C}$, for the left and caster wheel chains, and $\theta_{1-4,r}$ for the right wheel chain with as rotations around the z axis using the notation defined in [19]. This provides two degrees of freedom needed to traverse the non-planar surface. Frame $\{S_i\}$ describes the climbing surface at the point of contact of wheel i and is located relative to $\{I\}$ through the transformation,

$$T^I_{S_i} = \begin{bmatrix} -s\phi_i & 0 & c\phi_i & r_c c\phi_i \\ c\phi_i & 0 & s\phi_i & r_c s\phi_i \\ 0 & 1 & 0 & z_i \\ 0 & 0 & 0 & 1 \end{bmatrix} \tag{4}$$
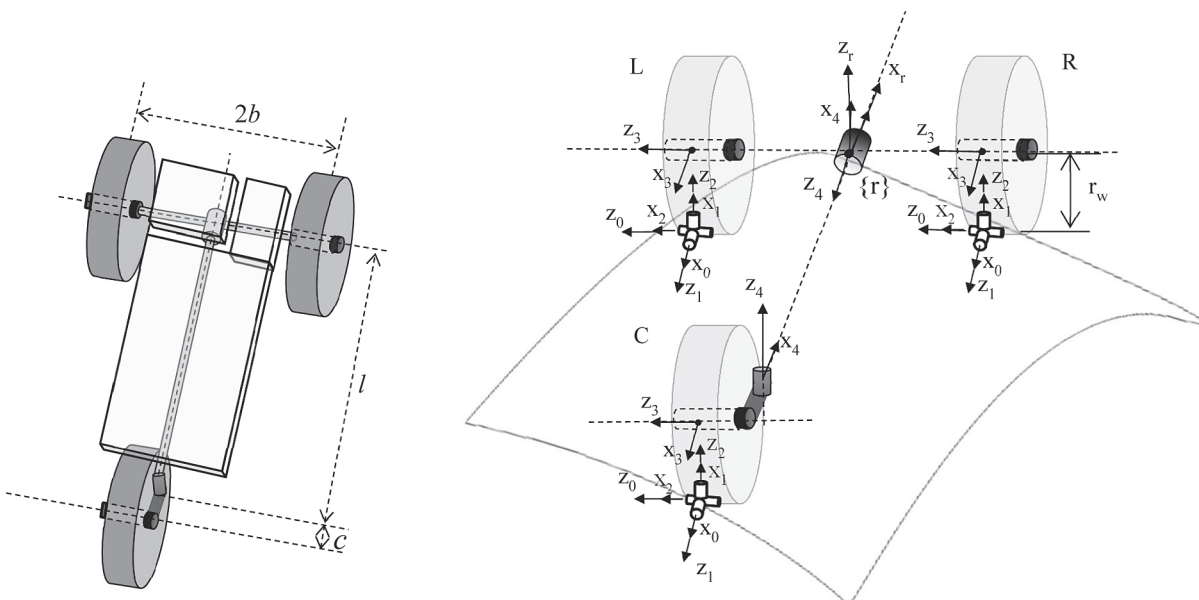
Fig. 2. Differential Steer System Platform and Kinematic Frame Assignments
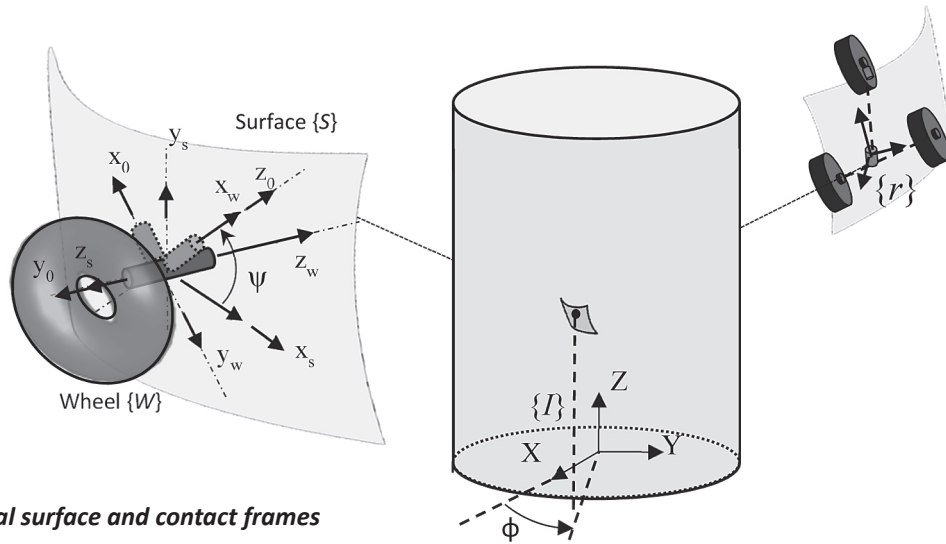
Fig. 3. Cylindrical surface and contact frames

where z_i and ϕ_i represent translation and rotation about the z axis of the inertial frame $\{I\}$, r_c is the radius of the cylinder, and subscript i refers to the three wheels, left, right or caster. Frame $\{W_i\}$ describes the wheel surface at the point of contact of each wheel located relative to $\{S_i\}$ through a rotation of ψ about the z axis of $\{S_i\}$:

$$R_{W_i}^{S_i} = \begin{bmatrix} c\psi & s\psi & 0 \\ s\psi & -c\psi & 0 \\ 0 & 0 & -1 \end{bmatrix} \qquad (5)$$

Note that in comparison with reference [18], frames $\{S_i\}$ and $\{W_i\}$ here are defined as outward normal frames to the surface and wheel bodies. Frame $\{0_i\}$ is defined as a fixed rotation relative to $\{W_i\}$ to represent the first joint in the wheel branch having an axis parallel to the wheel axis and intersecting the contact point:

$$R_{0_i}^{W_i} = \begin{bmatrix} 0 & 0 & 1 \\ -1 & 0 & 0 \\ 0 & -1 & 0 \end{bmatrix}. \qquad (6)$$

Thus the transformation of each wheel to the inertial frame is given as:

$$T_{0_i}^I = \begin{bmatrix} s\phi_i s\psi & c\phi_i & -c\psi s\phi_i & r_c c\phi_i \\ -c\phi_i s\psi & s\phi_i & c\phi_i c\psi & r_c s\phi_i \\ c\psi & 0 & s\psi & z_i \\ 0 & 0 & 0 & 1 \end{bmatrix}. \qquad (7)$$

Note that this transformation is a function of the three parameters, z_i, ϕ_i, and ψ_i. A set of differential equations are constructed to propagate the position and orientation of the contact frames forward in time in the following manner. The instantaneous kinematics are used to describe the velocity state of the entire system; this yields the instantaneous velocity of frame $\{W_i\}$ with respect to $\{S_i\}$, for $i = L, R, C$. The method presented by Montana, [18], is used to develop a set of differential equations which are used to describe the motion of frames $\{W_i\}$ and $\{S_i\}$. The parameters, z_i, ϕ_i and, ψ_i are then described as a function of time

and can be integrated. Finally, the robot configuration is updated in time as the wheel contacts move along the surface. This update is based on satisfying the constraints contained in the instantaneous kinematic model. Finally, a strategy to implement this with a kinematic control scheme is presented.

Returning to the robot kinematics, the length and width of the robot is denoted as l and $2b$ respectively and are shown in Figure 2. The wheels are assumed toroid in shape (but other shapes could be selected) with outer radius r_o and inner radius, r_{in}, with caster offset, c, for the steering wheel. A set of three homogenous transformations, one associated with each wheel chain, $\mathbf{T}_{O_L}^r, \mathbf{T}_{O_R}^r$ and $\mathbf{T}_{O_C}^r$ and three Jacobian matrices are used to relate the velocity of the robot chassis $\{r\}$ to the configuration state velocity for each wheel branch as:

$$\mathbf{v}_r = \mathbf{J}_L \dot{\mathbf{q}}_L = \mathbf{R6}_{0_R}^{0_L} \mathbf{J}_R \dot{\mathbf{q}}_R = \mathbf{R6}_{0_C}^{0_L} \mathbf{J}_C \dot{\mathbf{q}}_C \qquad (8)$$

where $\dot{\mathbf{q}}_i = [\dot{\theta}_1 \quad \dot{\theta}_2 \quad \dot{\theta}_3 \quad \dot{\theta}_4 \quad \dot{\theta}_5]_i^T$ is the vector of joint parameters for wheel branch $i = L, R, C$ with $\dot{\mathbf{q}}_i$ containing $\dot{\theta}_{1-5}$ for $i = L, C$, and $\dot{\mathbf{q}}_i$ containing $\dot{\theta}_{1-4}$ for $i = R$, and

$$\mathbf{R6}_{0_R}^{0_L} = \begin{bmatrix} \mathbf{R}_{0_R}^{0_L} & \mathbf{0} \\ \mathbf{0} & \mathbf{R}_{0_R}^{0_L} \end{bmatrix}, \mathbf{R6}_{0_C}^{0_L} = \begin{bmatrix} \mathbf{R}_{0_C}^{0_L} & \mathbf{0} \\ \mathbf{0} & \mathbf{R}_{0_C}^{0_L} \end{bmatrix} \qquad (9)$$

with $\mathbf{R}_{0_R}^{0_L}, \mathbf{R}_{0_C}^{0_L}$ the adjoint transformations that project velocity in $\{0_R\}$ and $\{0_C\}$ into velocity in $\{0_L\}$. The velocity $\mathbf{v_r}$ must lie in the column space of $\mathbf{J}_L, \mathbf{R6}_{0_R}^{0_L} \mathbf{J}_R$ and $\mathbf{R6}_{0_C}^{0_L} \mathbf{J}_C$ as shown in Equation 8. A singular value decomposition is performed on each of these matrices yielding $\mathbf{J}_L = \mathbf{U}_L \mathbf{\Sigma}_L \mathbf{V}_L$, $\mathbf{R6}_{0_R}^{0_L} \mathbf{J}_R = \mathbf{U}_R \mathbf{\Sigma}_R \mathbf{V}_R$ and $\mathbf{R6}_{0_C}^{0_L} \mathbf{J}_C = \mathbf{U}_C \mathbf{\Sigma}_C \mathbf{V}_C$ where the columns of $\mathbf{U}$ are the left singular vectors of the corresponding Jacobian. Each $\mathbf{U}$ matrix is further partitioned as $\mathbf{U}_L = [\mathbf{U}_{L1} \ \mathbf{U}_{L2}]$, $\mathbf{U}_R = [\mathbf{U}_{R1} \ \mathbf{U}_{R2}]$ and $\mathbf{U}_C = [\mathbf{U}_{C1} \ \mathbf{U}_{C2}]$ where $\mathbf{U}_{L2}, \mathbf{U}_{R2}, \mathbf{U}_{C2}$ correspond to the zero singular values in each decomposition, representing the left null space of $\mathbf{J}_L, \mathbf{R6}_{0_R}^{0_L} \mathbf{J}_R$ and $\mathbf{R6}_{0_C}^{0_L} \mathbf{J}_C$, and are of size $6 \times 1, 6 \times 2$ and 6×1 respectively. This leads to a total of four constraints derived from Equation 8 as,

$$U_{L2}^T \mathbf{v}_r = 0; \ U_{R2}^T \mathbf{v}_r = 0; \ U_{C2}^T \mathbf{v}_r = 0; \quad (10)$$

Two components of $\mathbf{v}_r$ are defined as the allowable two dof inputs of the robot (these must be consistent with the four constraints) to then solve for $\mathbf{v}_r$ from the four constraint equations. This allows configuration velocities $\dot{\mathbf{q}}_i$, $i = L, R, C$ to be solved making use of the Moore-Penrose inverse function as,

$$\dot{\mathbf{q}}_L = \mathbf{J}_L^{+}\mathbf{v}_r; \ \dot{\mathbf{q}}_R = (\mathbf{R6}_{0_R}^{0_L}\mathbf{J}_R)^{+}\mathbf{v}_r; \ \dot{\mathbf{q}}_C = (\mathbf{R6}_{0_R}^{0_L}\mathbf{J}_C)^{+}\mathbf{v}_r. \ (11)$$

These equations assume wheel contact locations (defined as the coordinates z_i and ϕ_i, $i=L, R, C$, Equation 4) and wheel headings (ψ_i, $i=L, R, C$, Equation 5) are fixed instantaneously and propagated forward in time according to a set of differential equations governing the contact as defined below. The joint parameters in the robot ($\mathbf{q}_i$) are found by satisfying the kinematic model shown in Figure 2 for a given set of contact points.

2.2 Contact Equations

The wheel contact locations are propagated forward in time using the method presented in [18]. This gives a set of differential equations that describe the motion of contact between the robot wheels and climbing surface. The surfaces are characterized through the function f with tangent directions, $f_u(\mathbf{U})$ and $f_v(\mathbf{U})$ the outward normal direction, $g(f(\mathbf{U}))$ at location $\mathbf{U}$ and the metric $\mathbf{M}$, curvature $\mathbf{K}$ and torsion $\mathbf{T}$ measures can be similarly found at each location $\mathbf{U}=[u, v]^T$ for both the wheel and the surface, [18]:

$$\mathbf{M} = \text{diag}(\|f_u(\mathbf{U})\|, \|f_v(\mathbf{U})\|) \quad (12)$$

$$\mathbf{K} = [x(\mathbf{U}), y(\mathbf{U})]^T[z_u(\mathbf{U})/\|f_u(\mathbf{U})\|, z_u(\mathbf{U})/\|f_v(\mathbf{U})\| \ ] \ (13)$$

$$\mathbf{T} = y(\mathbf{U})^T[x_u(\mathbf{U})/\|f_u(\mathbf{U})\|, x_v(\mathbf{U})/\|f_v(\mathbf{U})\| \ ] \quad (14)$$

Where $x(\mathbf{U}) = f_u/\|f_u(\mathbf{U})\|$, $y(\mathbf{U}) = f_v/\|f_v(\mathbf{U})\|$, and $z(\mathbf{U}) = x(\mathbf{U}) \times y(\mathbf{U})$. The contact equations are given for the contact point motion on the wheel, $\dot{\mathbf{U}}_W = [\dot{u}_W \ \dot{v}_W]^T$, and the motion of the contact point on the climbing surface, $\dot{\mathbf{U}}_S = [\dot{u}_S \ \dot{v}_S]^T$ as

$$\dot{\mathbf{U}}_W = \mathbf{M}_W^{-1}(\mathbf{K}_W + \widetilde{\mathbf{K}_S})^{-1} \left(\begin{bmatrix} -\omega \ y \\ \omega \ x \end{bmatrix} - \widetilde{\mathbf{K}_S} \begin{bmatrix} v_x \\ v_y \end{bmatrix} \right) \quad (15)$$

$$\dot{\mathbf{U}}_S = \mathbf{M}_S^{-1}\mathbf{R}_W^S(\mathbf{K}_W + \widetilde{\mathbf{K}_S})^{-1} \left(\begin{bmatrix} -\omega \ y \\ \omega \ x \end{bmatrix} - \mathbf{K}_W \begin{bmatrix} v_x \\ v_y \end{bmatrix} \right) (16)$$

$$\dot{\psi} = \omega \ z + \mathbf{T}_W \mathbf{M}_W \dot{\mathbf{U}}_W + \mathbf{T}_S \mathbf{M}_S \dot{\mathbf{U}}_S \quad (17)$$

where $\dot{\psi}$ is the rotation between the wheel and surface frames about the common normal, $R_\psi = R_W^S$ is the orientation of the wheel frame projected on the surface frame as given in Equation 5, $\widetilde{K_S}$ is the curvature of surface relative to the wheel at the point of contact given as,

$$\widetilde{\mathbf{K}_S} = \mathbf{R}_W^{S \ T}\mathbf{K}_S\mathbf{R}_W^S \quad (18)$$

And $[-\omega_y \ \omega_x]^T = [-\omega_{y_W} \ \omega_{x_W}]^T = [-\mathbf{q}(2) \ \mathbf{q}(1)]^T$ the relative rotational velocities and $[-v_x \ v_y]^T = [v_{x_W} \ v_{y_W}]^T = [0 \ 0]^T$ due to the no-slip wheel assumptions and $\mathbf{q}(i)$ is the ith component of vector $\mathbf{q}$. It must be noted that the subscript i has been removed in the preceding equations, however each operation is performed for each of the three wheels. Equations 15–17 represent five equations each for the three wheels, $i=L, R, C$ or 15 equations in total to solve for the contact point velocities along the wheel and climbing surface. The parameters $\dot{\mathbf{U}}_W$, $\dot{\mathbf{U}}_S$ define the contact parameters from Equation 4 as:

$$\dot{\phi} = \frac{\dot{\mathbf{U}}_S(1)}{r_c} = \frac{\dot{u}_S}{r_c} \quad (19)$$

and

$$\dot{z} = \dot{\mathbf{U}}_S(2) = \dot{v}_S \quad (20)$$

where subscript i is removed such that Equations. 12–20 apply to all three wheels.

2.3. Update and Recursion

The kinematic constraints are a function of the robot configuration as seen in Equation 10. These configuration parameters must be updated with the surface geometry as the robot navigates along the climbing surface. This procedure begins by updating the contact point between the wheel and the surface. This is performed for each wheel and is updated based on the integration of Equations 19 and 20 and assumed coincident with $\mathbf{U}_{Oi}$. The locations of these contact points on the cylindrical climbing surface are described in the inertial frame as,

$$\mathbf{U}_{S_i} = [r_c * \cos(\Phi_i) \ r_c * \sin(\Phi_i) \ z_i]^T \quad (21)$$

Two defined inputs, $\mathbf{q}_L(4)$ and $\mathbf{q}_R(4)$, are calculated from integrating appropriate terms in Equation 11, with the remaining 12 configuration parameters in $\mathbf{q}_L$, $\mathbf{q}_R$, and $\mathbf{q}_c$ determined as the set satisfying the equality of the homogenous transformations. These transformations are used to define the position and orientation of frame {r} onto the inertial frame {I} for each of the three wheel branches,

$$\mathbf{T}_{rOL}^I = \mathbf{T}_{rOR}^I = \mathbf{T}_{rOC}^I \quad (22)$$

It is important to note that several solutions should be available in each branch, however the desired solution is closest to the original configuration and is expected to remain in a relatively nearby region. This process is solved numerically using the MATLAB FSOLVE function which requires an initial guess (previous position).

2.4. Kinematic Control

Based on the model given, a control strategy is demonstrated based on an incremental control about a reference trajectory, [20]. Here, the goal is to drive the robot to travel along a specified reference trajectory defined by tracking an idealized, virtual robot that

returns a desired reference position $[X_{ref}\ Y_{ref}\ \theta_{ref}]$ at each update cycle, both described in the inertial frame. The current error in position is first determined in Cartesian coordinates:

$$\Delta X = X_{ref} - X_{current} \qquad (23)$$

$$\Delta Y = Y_{ref} - Y_{current} \qquad (24)$$

and then cast into a coordinate frame that defines the error in terms of distance (ρ), direction to reference position (α), and direction to reference orientation (β).

$$\rho = \sqrt{\Delta X^2 + \Delta Y^2} \qquad (25)$$

$$\alpha = atan2(\Delta Y, \Delta X) \qquad (26)$$

$$\beta = \theta_{ref} - \left(\psi_L - \frac{\pi}{2}\right) - \alpha \qquad (27)$$

A linear control scheme is now defined in the robot local frame as,

$$v_x = K_p * \rho \qquad (28)$$

$$\omega_z = K_\alpha * \alpha + K_\beta * \beta \qquad (29)$$

which form the two velocity inputs for **v**$_r$. As given in Siegwart and Nourbakhsh [20], stability of this linearized control system is shown to exist when K_p>0, K_β>0, and K_α-K_p>0.

3. Implementation

The model demonstrated above is implemented in MATLAB for simulation and design purposes as described in this section. This initial value problem is solved via numerical integration using MATLAB's ODE 45 solver. The desired path is defined in one of two methods; open loop, specifying desired robot velocity, or closed loop, specifying a desired reference trajectory. The geometric parameters for the climbing surface and robot wheels are first defined through **M**$_S$, **K**$_S$, **T**$_S$, and **M**$_W$, **K**$_W$, **T**$_W$. Second, the initial conditions are then defined for the robot through the initial wheel contact locations, $[\phi_i\ z_i\ \psi_i]$, i=L, R, and C, and wheel branch configuration vectors **q**$_L$, **q**$_R$, **q**$_C$. The robot frame velocity (**v**$_r$) inputs are specified through v_x and w_z, with remaining terms solved through Equation 10. The configuration parameter velocities are solved using Equation 11. The necessary information to solve for the contact point velocities is now available and solved using Equations 15–17. The new contact points are updated and used to solve for the new configuration state using the MATLAB FSOLVE function. This Function solves for a set of parameters minimizing the objective F defined as

$$F = \mathbf{f}(\vec{q}_L, \vec{q}_R, \vec{q}_C)^T \mathbf{f}(\vec{q}_L, \vec{q}_R, \vec{q}_C) \qquad (30)$$

with $\mathbf{f} = [\mathbf{T}_L^I(i,j) - \mathbf{T}_R^I(i,j); \mathbf{T}_L^I(i,j) - \mathbf{T}_C^I(i,j)]^T$ for matrix elements (i,j) = (1,4), (2,4), (3,4), (1,3), (2,3), (3,1). This function represents equality between three homogenous transformations that connect the wheel

contact points to the robot frame origin. The time step is advanced and the function is implemented at each updated time step with the process repeating using current velocity inputs. This approach is used in the validation and application sections below.

4. Model Validation

The model is validated first through a comparison with a simplified analytical solution and then through tests using a lab-based prototype robot. The analytical comparison proceeds first by evaluating a reduced system permitting closed-form solutions to the path of the contact point along the climbing surface. The reduced system assumes that the robot is performing a circular move with one wheel, spherical instead of toroidal, fixed and the other rotating such that the moving wheel is pivoting about a fixed point, yielding the following set of differential Equations:

$$\dot{\psi}_{rs} = \omega_z \qquad (31)$$

$$\phi_{rs} > 0 \qquad (32)$$

and

$$z_{rs} = \sqrt{L^2 - r_w{}^2 + (r_c{}^2 - r_w r_c)(\cos(\phi_i) - 1)} \qquad (33)$$
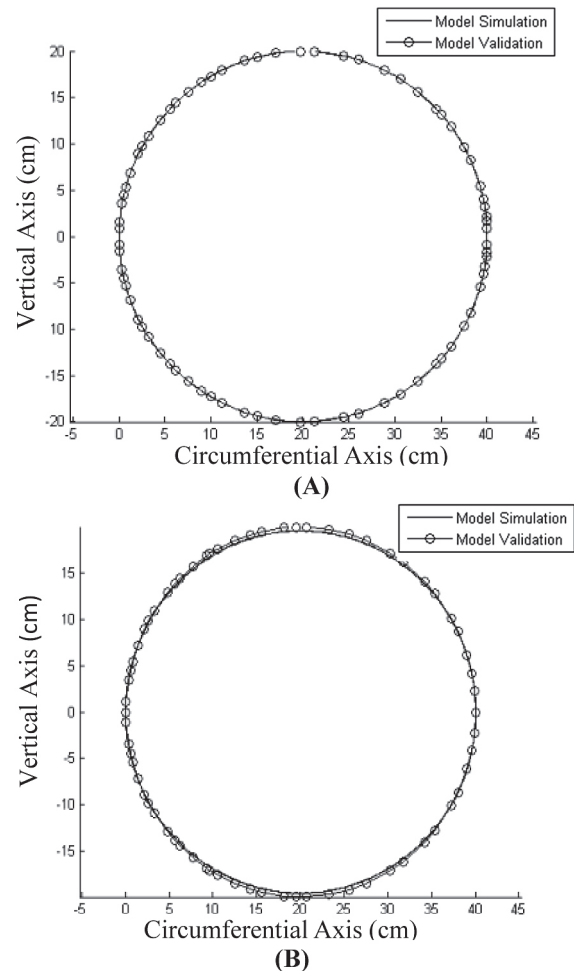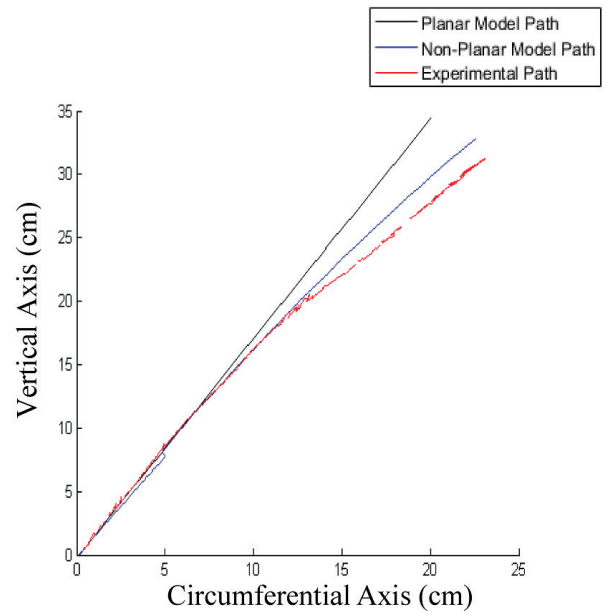

Fig. 4. Comparing Model over: (A) Large Radius Cylinder and (B) Smaller Radius Cylinder

Fig. 5. Prototype Climbing Robot Navigating Cylindrical Tank


Fig. 6. Comparison of Model and Prototype Test

where $L = \sqrt{r_w^2 + 4b^2}$, is the length from the pivot point to the center of the spherical wheel; with r_w the wheel radius, r_c the surface cylinder radius, and b is half the width of the robot as seen from Figure 2 above. The model above is simulated to execute a path in which the contact point of one wheel is held fixed while the other travels around it and the results are compared with those from the reduced system model. This is shown for a robot of dimensions of $r_w = 0.05$ m, $b = 0.10$ m and over two cylinder sizes, $r_c = 1e5$ m (nearly planar, Figure 4a) and $r_c = 200$ m (Figure 4b).

The comparisons between the two models indicate generally good correlation with the analytical results with a maximum square error of 1.8e-3 m for the case shown in Figure 4b. Discrepancies between the model and the reduced solution are in part caused by the assumed spherical wheel on the reduced system.

The proposed model is now validated with experimentally-derived data to evaluate its validity. To perform the experimental tests, a differential-steer mobile robot climbing system is constructed for operating on non-planar surfaces. The robot chassis
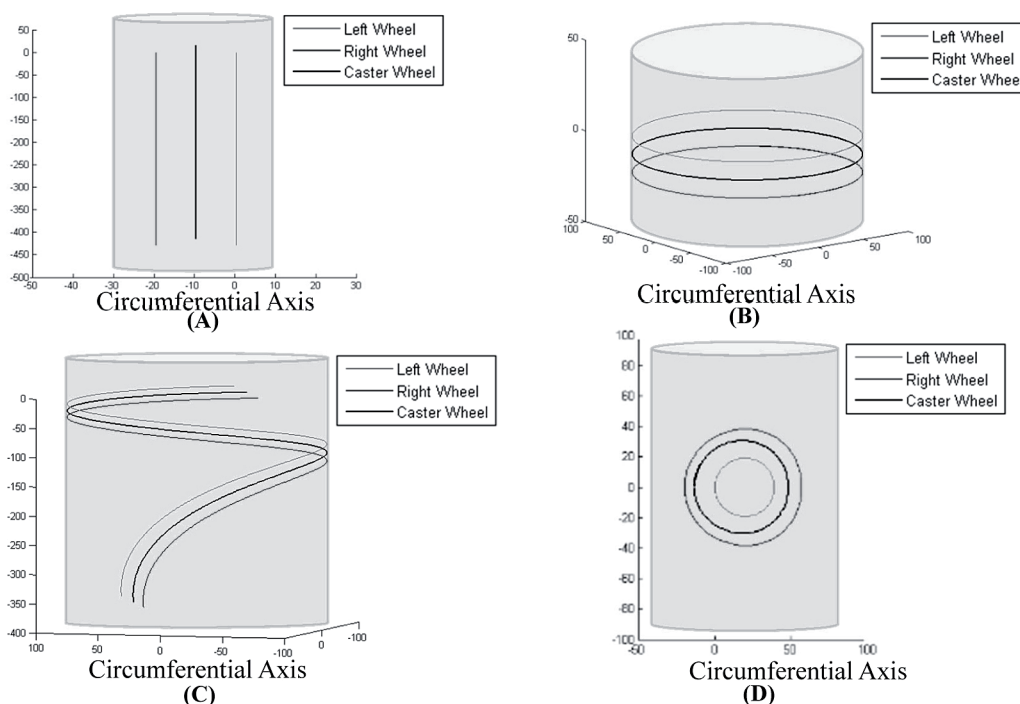
Fig. 7. Evaluating Four Maneuvers on Cylindrical Surface; A) Vertical Path B) Horizontal Path C) Spiral Path D) Circular Path

was 3D printed and contains two magnetic wheels and a passive caster wheel providing stability for the platform. The two magnetic wheels are mechanically coupled to ensure known, equal inputs of the left and right drive wheels. The prototype test robot is shown in Figure 5 and has kinematic parameters as follows: $2b$ = 0.1016 m, l = 0.04445 m, = 0.0254 m. The climbing surface is a cylindrical tank with r_c = 0.381 m and uniform surface properties leading to consistent friction characteristics. The prototype of this system was developed so that straight line motion along a non-planar, (cylindrical), surface could be determined and compared to model results. The motion of the climbing robot is monitored using an OptiTrack motion capture system consisting of eighteen cameras oriented so that the entire testing workspace, (robot and climbing surface), is visually monitored. The motion capture system can achieve a sub millimeter accuracy based on the calibration of the system. This ensures measurements are accurate while testing on non-planar surfaces. The ground plane is located with the Z axis aligned with the center of the cylindrical climbing surface and the X and Y plane lying at one end of the cylinder. The climbing robot carries reflective markers so that its position and orientation are measured as it traverses the cylindrical climbing surface for comparison with the proposed model. The robot travels over a portion of the cylinder with equal left/right wheel velocities (enforced through a mechanical connection) and the results are shown in Figure 6 which presents and compares three paths as trajectories mapped onto the unwrapped cylinder surface. The black path represents the straight line travel that would be expected if using a planar model (assumes non-planar effects are small) while the red line shows the path obtained from the measured experimental data. The blue line represents the predicted results generated from the model using known robot and surface parameters. Figure 6 clearly shows that the planar assumption is not valid for this example and shows a strong correlation between the model and experimental data. It should be noted that the cylindrical surface had some feature defects (pitting, which was not considered in the model) and this caused the discontinuities in the experimental data. The results of this experimental comparison indicate the model is a useful predictive tool in the estimation of robot trajectory on cylindrical climbing surfaces.

5. Application

Using the model defined above, a series of robot maneuvers are considered on the cylindrical climbing surface. The first case considers four maneuvers that represent paths common for welding or inspection tasks. The second case demonstrates potential effects on a simulated path due to a change in the scale between the cylinder radius (r_c) and robot size (b). The final case demonstrates use of kinematic control to follow a predefined path. In all cases, the application results are demonstrated as paths traced by the contact point (of one or more robot wheels) on the climbing surface.

### Case 1: Robot Maneuvers on a Cylindrical Climbing Surface

The first case considers four different maneuvers of the robot on a single cylinder shown in Figure 7 a-d. Each maneuver is defined as set of constant, open-loop kinematic commands defined in the robot frame. With ratio of the surface curvature to half the width of the robot, (r_c/b), of 20. Figure 7 displays the paths of the Left, Right and Caster Wheel contact locations on the cylindrical climbing surface. The first maneuver, Figure 7a, directs the robot to operate vertically along the cylinder with the second maneuver directed horizontal (around the circumference of the cylinder, Figure 7b). Next, the robot performs maneuvers while oriented 45º from the surface, Figure 7c. The final maneuver yields a circular path by operating at a constant and nonzero linear and angular velocity, Figure 7d.

Case 2: Robot Maneuvers on Cylinders of Varying Radius

The second case demonstrates the potential effects of the non-planar surface on the robot path. This is considered by observing a generally circular path performed on varying cylinder sizes. The size of the cylindrical climbing surfaces ranges from essentially planar (large radius) to small (radius approaching robot width). This is performed by varying the scale between the cylinder radius (r_c) and the width of the robot ($2b$). The velocity inputs are selected for this maneuver providing a contractible closed-path as shown in Figures 7d and 8. Figure 8 displays theses maneuver performed on cylinders of radius varying from r_c = 2e5 m, 2e2 m, and 0.5e2 m. The results are presented as a planar sheet produced by unwrapping the cylinder surface which displays as the cylinder radius decreases, the paths remain closed but becomes increasingly oblong.

Case 3: Robot Maneuvers Using Kinematic Control

The third case considers kinematic control for three maneuvers considered common in manufacturing environments. A ratio, surface curvature to half the width of the robot (r_c/b), of 20 was utilized for testing this method of control. These tasks are rep-
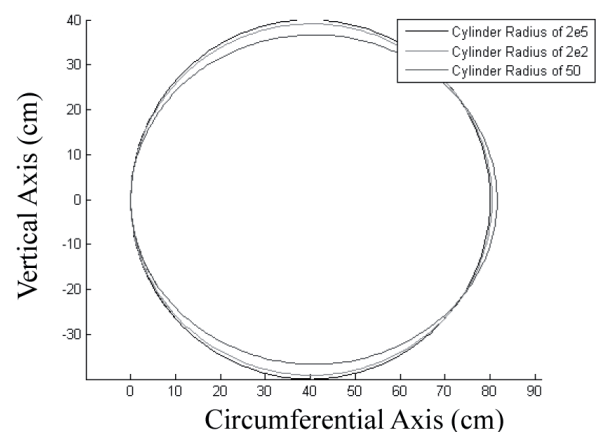
Fig. 8. Robot Paths for a Circular motion over Cylinders of Varying Radii
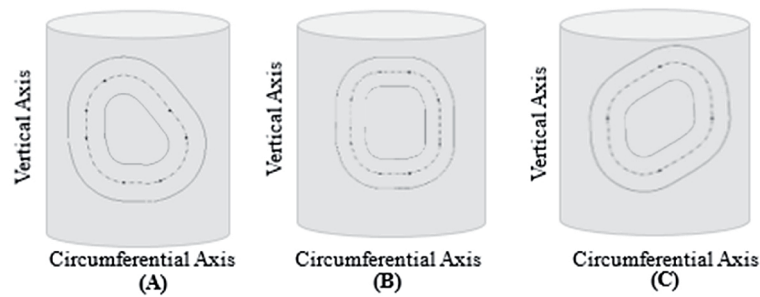
Fig. 9. Demonstrating Closed loop control over. A) Triangular Path, B) Square Path, C) Diamond Path

resentative of welding along an uneven surface and generally result in a path resembling a triangular, diamond or square. The paths generated in this section are guided by means of a kinematic controller to navigate along a specified path. The results are shown in Figures 9a–c, representing each wheel path and demonstrating the model is able to generally follow the desired path. The model results in closed-paths indicating its robustness and suitability to the chosen numerical integrator.

6. Discussion and Conclusion

The method discussed in this paper is used to evaluate mobile robot trajectory when moving over an uneven surface. Geometric representations of the contact point between two surfaces yield a set of ordinary differential equations and when combined with kinematic constraints these equations are solved in an iterative manner to describe the robot motion. The method is applied to a cylindrical climbing surface and a platform modeled as a three-wheeled differential-steer robot with toroid-type wheels. The objective of this work is to provide the groundwork for kinematic path planning of mobile robots that traverse known surfaces in order to perform manufacturing tasks such as inspection and welding.

The method constructed satisfies the no-slip constraints, ($v_x = v_y = 0$), which are assumed to be zero for this particular robot model. A set of kinematic constraints are developed using Equation 8 and are used to solve for the velocity of the robotic platform, (v_r). Once the robot velocity is determined the joint velocities are then determined using Equation 8. The no-slip assumption combined with the joint velocities allow the implementation of Equations 15–17, [18], allowing for updated contact points on the climbing and wheel surfaces. Equations 15–17 also provide an updated orientation of the wheel frames relative to the surface frame. The model formulation satisfies similar constraints as seen in, [14]; however the current model prescribes the velocity vector at the geometric center of the robot, in the robot frame, with the kinematic constraints stated in terms of this velocity. The model was validated through numeric as well as experimental testing. The numerical evaluation is performed using a simplified analytical representation of the model expressed using Equations 31–33. The results of this comparison (Figure 4 a–b) show the model consistently represents a purely

circular path for larger radius climbing surface and paths that are oblong in nature for smaller radius cylinders. The model was additionally validated through empirical testing with a differential steer robot climbing on a small cylindrical tank. The empirical tests and corresponding model applications clearly show the significance of curvature on robot kinematic position estimates as the cylinder radius is reduced relative to the size of the robot. When considering a non-dimensionalized ratio of the surface curvature to half the width of the robot, (r_c/b), operational conditions in which the curvature to robot ratio is 15 or less show noticeable error when relying on the planar assumption. This is observed in application case two in which a robot operating on a smaller radius cylinder (surface curvature to robot ratio of 13.3) demonstrates a noticeable departure in the predicted path when compared with a planar-assumption (surface curvature to robot ratio of >500). This is similarly observed in the empirical example, here where a small robot on a small tank (surface curvature to robot ratio of 7.5) operates with a nominal straight line input where both wheels are driven at an equal constant speed, but travels along a path that is a curved line when viewed on the unwrapped surface of the tank.

The non-planar kinematic model can be used to improve robot kinematic estimates for applications in which the surface curvature to robot ratio is at or below a certain threshold. The model can be implemented as part of a kinematic control scheme, as shown in application case three, to track desired trajectories on curved surfaces. This example demonstrates an open-loop implementation of the kinematic control law relying on the non-planar kinematic model for current estimates of the robot position on the cylinder surface. This non-planar kinematic model could also be combined with external sensing capabilities as an improved prediction step to enable improved performance when performing manufacturing tasks on non-planar surfaces.

AUTORS

Joshua Qualls*, Stephen Canfield, Alexander Shibakov – Tennessee Technological University, Cookeville, Tn. USA.

*Corresponding author

REFERENCES

[1] O'Toole A., Canfield S. L., "Developing a Kinematic Estimation Model for a Climbing Mobile Robotic Welding System". In: *Proc. of the 2010 ASME International Design Engineering Technical Conferences*, Montreal Quebec, Canada, 15–18 Aug. 2010, DETC2010-28878.

[2] Canfield S. L., Beard J. W., "Robotic inspection in power plants", *ISA 51st Annual Instrumentation Symposium*, 2005.

[3] Mandow A., Martínez J. L., Morales J., *et al.*, "Experimental kinematics for wheeled skid-steer mobile robots". In: *IEEE/RSJ International Conference on Intelligent Robots and Systems, IROS 2007*. DOI: 10.1109/IROS.2007.4399139.

[4] Wong J. Y., Huang W., "Wheels vs. tracks–A fundamental evaluation from the traction perspective", *Journal of Terramechanics*, vol. 43, no. 1, 2006, 27–42.

[5] Wong J. Y., Chiang C., "A general theory for skid steering of tracked vehicles on firm ground". In: *Proceedings of the Institution of Mechanical Engineers, Part D: Journal of Automobile Engineering*, vol. 215, no. 3, 2001, 343–355.

[6] Martínez J. L,. Mandow A., Morales J., Pedraz S., Garcia-Cerezo A., "Approximating kinematics for tracked mobile robots", *The International Journal of Robotics Research*, vol. 24, no. 10, 2005, 867–878. DOI: 10.1177/0278364905058239.

[7] Shiller Z., Hua M., "Trajectory planning of tracked vehicles". In: *Proceedings – 1993 IEEE International Conference on Robotics and Automation.* DOI: 10.1109/ROBOT.1993.292242.

[8] Kozłowski K., Pazderski D., "Modeling and control of a 4-wheel skid-steering mobile robot", *Int. J. Appl. Math. Comput. Sci.*, vol. 14, no. 4, 2004, 477–496.

[9] Caracciolo L., De Luca L., "Trajectory tracking control of a four-wheel differentially driven mobile robot". In: *Proceedings. 1999 IEEE International Conference on Robotics and Automation,* vol. 4. DOI: 10.1109/ROBOT.1999.773994.

[10] Song X., Seneviratne L.D., Althoefer K., Song Z., "A robust slip estimation method for skid-steered mobile robots". In: *10th International Conference on Control, Automation, Robotics and Vision, ICARCV 2008*. DOI: 10.1109/ICARCV.2008.4795532.

[11] Yu W., Chuy O., Collins E., Hollis P., "Analysis and Experimental Verification for Dynamic Modeling of A Skid-Steered Wheeled Vehicle", *IEEE Proceedings on Robotics*, vol. 26, no. 2, April 2010.

[12] Sarkar N., Kumar V., "Control of Mechanical Systems With Rolling Constraints Application to Dynamic Control of Mobile Robots", *The International Journal of Robotics Research*, vol. 13, no. 1, 1994, 55–69.

[13] Sarkar N., Yun X., Kumar V., "Dynamic Control of 3-D Rolling Contacts in Two-Arm Manipulation", *IEEE Transactions on Robotics and Automation,* vol. 13, no. 3, 1997, 364–376.

[14] Chakraborty N., Ghosal A., "Kinematics of wheeled mobile robots on uneven terrain", *Mechanism and Machine Theory*, vol. 39, no. 12, 2004, 1273–1287. DOI: 10.1016/j.mechmachtheory.2004.05.016.

[15] Davis P.W., Sreenivasan S.V., Choi B.J., "Kinematics of Two Wheels Joined By A Variable Length Axle on Uneven Terrain". In: *ASME 1997 International Design Engineering Technical Conferences*, DETC97/DAC-3857, Sacramento, 14–16 Sept. 1997.

[16] Sreenivasan S. V., Nanua P., "Kinematic Geometry of Wheeled Vehicle Systems". In: *24th ASME Mechanisms Conference*, 96-DETC-MECH-1137, Irvine, CA, 1996.

[17] Auchter J., Moore C. A., Ghosal A., "A novel kinematic model for rough terrain robots", *Advances in Computational Algorithms and Data Analysis*, Springer Netherlands, 2009, 215–234. DOI: 10.1007/978-1-4020-8919-0_16.

[18] Montana D.J., "The kinematics of contact and grasp", *Int. J. Rob. Res.*, vol. 7, no. 3, ,1988, 17–32.

[19] Spong M., Vidyasagar M., *Robot modeling and control*, New York: John Wiley & Sons, 2006.

[20] Siegwart, R. and Nourbakhsh, I. *Intro to Autonomous Mobile Robots*. MIT press, 2004.